

3D Gaussian Splatting with Normal Information for Mesh Extraction and Improved Rendering

Meenakshi Krishnan
Mathematics, Univ. of Maryland,
College Park, USA
mkrishn9@umd.edu

Liam Fowl
Google, New York, USA
lfowl@google.com

Ramani Duraiswami
Computer Science & UMIACS, Univ. of Maryland
College Park, USA
ramanid@umd.edu

Abstract—Differentiable 3D Gaussian splatting has emerged as an efficient and flexible rendering technique for representing complex scenes from a collection of 2D views and enabling high-quality real-time novel-view synthesis. However, its reliance on photometric losses can lead to imprecisely reconstructed geometry and extracted meshes, especially in regions with high curvature or fine detail. We propose a novel regularization method using the gradients of a signed distance function estimated from the Gaussians, to improve the quality of rendering while also extracting a surface mesh. The regularizing normal supervision facilitates better rendering and mesh reconstruction, which is crucial for downstream applications in video generation, animation, AR-VR and gaming. We demonstrate the effectiveness of our approach on datasets such as Mip-NeRF360, Tanks and Temples, and Deep-Blending. Our method scores higher on photorealism metrics compared to other mesh extracting rendering methods without compromising mesh quality.

Index Terms—Gaussian splatting, mesh reconstruction, signed distance function, novel-view synthesis

I. INTRODUCTION

Differentiable 3D Gaussian Splatting (GS) [1] has recently supplanted NERFs [2] as the preferred tool in rendering and reconstruction due to its low latency and accurate reconstructions. GS represents scenes using Gaussian primitives whose parameters—means, covariances, colors, and opacities—can be directly optimized using a differentiable training-free pipeline well adapted for GPU implementation, enabling real-time, highly realistic rendering without the computational expense of neural network-based volumetric renderings.

A primary application of GS is in novel-view synthesis - a technique to generate novel viewpoints of a 3D scene, given a set of 2D images. Since its introduction, it has inspired a plethora of works such as 4D Gaussian splatting for dynamic scene rendering [3], 3D content creation [4], human avatar modeling [5], and in text to 3D scene generation [6]. Through view synthesis, GS-generated scenes also potentially offer a valuable source of photorealistic, synthetic images for training generative AI models, including diffusion models and GANs. It can enable practitioners to create virtually unlimited training datasets, encompassing a broad spectrum of viewpoints and scene variations. Surface mesh extraction from rendered 3D scenes is also crucial for many downstream tasks in graphics.

In generative applications, surface mesh extraction can allow further manipulation of scenes beyond creating novel views, by aiding in editing, sculpting, and animating, all while maintaining temporal consistency. The explicit 3D representation enables object manipulation, viewpoint changes, and lighting adjustments while maintaining occlusion. Geometrically accurate rendering is also relevant in AR-VR applications and in gaming for accurate 3D scene reconstruction.

However, extracting the surface of the scene optimized via GS can be a challenge. This is because the Gaussian parameters evolve solely based on optimization of photometric losses, and may fail to accurately learn the underlying scene physical geometry. To achieve high-fidelity scene reconstruction, GS employs a densification process that significantly increases the number of Gaussians, often reaching several million 3D Gaussians with different scales and rotations, and overfits to reduce photometric error. The majority of these Gaussians are highly localized in order to enable accurate rendering of fine details and textures. This leads to a density function (whose level set describes the scene surfaces) being mostly zero everywhere, making it challenging for Marching Cubes [7] to generate accurate level sets, even with a high-resolution grid [8].

Thus, developing effective techniques to guide Gaussian splatting for geometrically accurate rendering that enables high-quality mesh generation is of crucial importance. Our main contribution is the development of a novel regularization method which removes the reliance on heuristic target functions, and compares gradients of an estimated signed distance function (SDF) with the monocular normals generated from training images via a pre-trained neural network. Pictured in Figure 1a is the effectiveness of our approach in guiding these gradients, resulting in much smoother, less noisy normals. Our method simultaneously produces scene representations that facilitate easy mesh extraction, while also improving the photorealism of novel views of the scene compared to existing works that also facilitate mesh generation for GS, and is demonstrated in several experiments.

II. RELATED WORK

A. Neural Rendering

Several approaches have applied deep learning techniques to the novel-view synthesis problem to varying degrees of

MK and RD are members of PIRL (Perceptual Interfaces and Reality Lab). They were supported by ONR Award N00014-23-1-2086 and a Dolby gift.

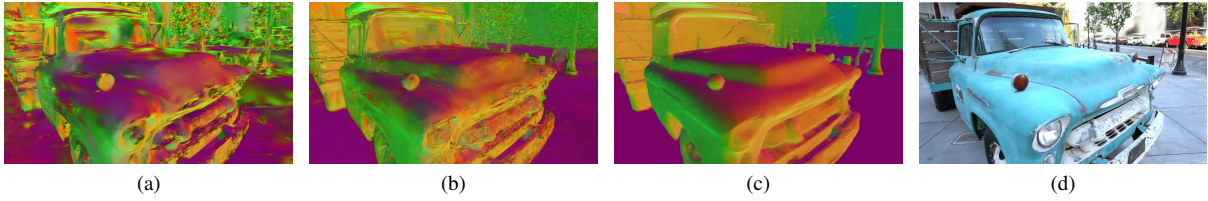


Fig. 1: Normals before (a) and after (b) optimization with our regularizer. Also depicted are ground truth normals (c) and the final rendered image (d). Constraining the SDF gradient to be the normal enables smoother geometric transitions in GS.

success [9]–[11]. Perhaps the most well known deep learning approach, Neural Radiance Fields (NeRF) [2], has garnered significant attention in the field of 3D scene reconstruction for its high quality rendering. In this method, 3D scenes are represented as continuous volumetric functions using multi-layer perceptrons (MLPs) which takes as inputs 3D positions and viewing directions, and outputs density and view-dependent colors for differentiable rendering. NeRF’s impressive rendering results come at the cost of higher latency due to the inclusion of large MLP layers. Several follow-up works have modified NeRF’s strategy to improve rendering quality, or decrease training time, with features like regularization terms [12], data-structures [13], or different encoders [14], [15].

Using a neural representation to parametrize the SDF of a 3D scene has also been the subject of various studies [16], [17]. Normal supervision using ground-truth normals [18], Eikonal loss [19] or incorporating properties of the SDF function such as the eigenvectors of its Hessian [20] as regularizing terms has recently gained attention as well. Our goal is to extend this approach to 3D GS.

B. Point-Based Rendering

Point-based rendering techniques represent 3D scenes as dense clouds of points, rather than polygons, relying on points to uncover underlying surface details. Such methods represents a different approach to the problem of novel-view synthesis that does away with deep learning pipelines and often instead focuses on other parametric approaches. In [21] a rasterizer renders points as one-pixel splats while a sphere-based scene representation is used in [22]. Differentiable 3D GS [1], based on the ideas proposed in [23], chooses Gaussian primitives whose parametrization naturally admits a differentiable volume representation, while also allowing fast rendering via α -blending. Various works have suggested further improvements such as anti-aliased rendering [24], improving the capability of rendering view-dependent effects [25], and compression and regularization [26], [27]. Other modern non deep learning approaches have also achieved impressive results producing photorealistic novel views. One popular example in the same vein as GS is plenoxels [28] which optimizes a spherical harmonics representation of a scene.

C. Mesh Representation

Another way of representing a scene is with a *mesh* that accurately describes surfaces and objects in it. As previously

detailed, mesh generation is crucial for several applications of scene rendering. However, both GS and NeRFs can struggle with mesh generation - but for different reasons.

For NeRFs, several mesh extraction techniques have been proposed, such as by embedding opacities and features into texture maps [29] or baking the neural fields into textures [30]. For the purposes of this work, we will focus on mesh extraction for GS. Since the standard 3D GS method does not explicitly encode any geometric information into the structure of the learned Gaussians, several works have tried to encode more geometric information into the GS process [8], [31], [32].

A distance-based Gaussian splatting technique for better mesh extraction was introduced in [33], while [34] suggests tightly binding the 3D Gaussian splats to meshes. In [8], a complex regularization method and an alternate strategy to extract meshes from the Gaussians were proposed. However, this often introduces *several* complex regularization terms - each with their own associated hyperparameters. It also comes at the cost of diminished performance on the photorealism front. One way to encode more geometric structure into the GS process is with *normal supervision*. Gao et al [35] propose using the gradients of rendered depths as pseudo-ground-truth for normal supervision. Closely related to our work is [31] where neural network estimated monocular normals are used to supervise the smallest scaling axis of a Gaussian that is encouraged to be flat to align with the surface.

III. METHOD

We follow the general pipeline as in the original Gaussian Splatting paper [1]. Like NeRF methods, the inputs are cameras calibrated with Structure-from-Motion (SfM) [36], and Gaussians are initialized using the sparse point cloud obtained. The 3D scene is represented by a large set of Gaussians, each parametrized by its mean μ , and covariance Σ :

$$G(x, y) = \exp\left(-\frac{1}{2}(x - \mu)^T \Sigma^{-1}(x - \mu)\right).$$

They are also associated with opacity coefficients $\alpha \in [0, 1]$ and spherical harmonics coefficients that represent the colors emitted by the Gaussians in all directions. These parameters are optimized during the training process. To ensure that the positive semi-definite property of the covariance matrices is retained during the optimization process, these matrices are parametrized using rotation and scaling matrices denoted as R and S , respectively with $\Sigma = RSS^T R^T$.

The 3D Gaussians are projected onto the 2D image plane as splats and blended using weighted sums of color and opacity. A fast tile-based rasterization method efficiently does the 3D-to-2D projection and applies α -blending which gives GS its main speed advantage over neural volumetric representations. The optimization is interleaved with adaptive density control of the Gaussians where more are added to both “empty” areas (with missing geometric features) and areas where a single Gaussian covers large parts of the scene. Essentially transparent Gaussians with opacities close to 0 are pruned between iterations.

For a given GS scene, [8] defines a corresponding density function at any space location p as sum of Gaussian values weighted by their alpha-blending coefficients,

$$d(p) = \sum_g \alpha_g \exp\left(-\frac{1}{2}(p - \mu_g)^T \Sigma_g^{-1} (p - \mu_g)\right). \quad (1)$$

They then propose a target density function that promotes flat and surface-aligned optimized Gaussians to supervise (1). To further increase surface alignment, they also define an ideal SDF function whose zero level sets correspond to the surface of the scene. To estimate the SDF for the current iteration, the depth maps of the Gaussians from the training viewpoints are used which can be rendered using the splatting rasterizer. Then for a point p visible from a training viewpoint, the estimated SDF $\hat{f}(p)$ at that point is taken to be the difference between the depth of p and the depth in the corresponding depth map at the projection of p . Additional regularization is applied for opacity, and the SDF gradient is pushed towards the direction of the smallest axis of the Gaussian.

Instead of a target SDF, we propose supervising the gradients of the SDF using its (unsigned) cosine similarity with the monocular normals obtained from a pretrained neural network such as Omnidata [37] or MiDaS [38]. First the gradients are projected into the camera space using the world-to-view transform, after which their values at the corresponding pixel positions are obtained using the GS rasterizer. Specifically, at a point p , denoting the rasterized gradient as $\nabla \hat{f}_p$ and the normals as n_p , we have a regularizing term of the form:

$$R(\hat{f}) = \sum_{p \in P} \frac{|\nabla \hat{f}_p \cdot n_p|}{\|\nabla \hat{f}_p\| \|n_p\|}. \quad (2)$$

Here P denotes the set of pixel points in the training images. Then for the regularizing iterations, the loss is taken to be

$$\mathcal{L} = \mathcal{L}_1 + \lambda_{\text{DSSIM}} \mathcal{L}_{\text{DSSIM}} + \lambda_r R(\hat{f}),$$

where \mathcal{L}_1 and $\mathcal{L}_{\text{DSSIM}}$ denote the standard L^1 norm loss and the D-SSIM term. We set $\lambda_{\text{DSSIM}} = 0.2$ and λ_r is tuned for the different scenes; a value between 0.1 and 0.4 works well. Additionally, we use entropy regularization for a short number of iterations to encourage the opacities to be binary, since we need the Gaussians to represent a surface and want to avoid semi-transparent ones. A mesh is extracted from the Gaussians obtained after optimization with the regularization terms by running a Poisson reconstruction [39] on points sampled on

TABLE I: Results on the MipNerf Dataset for indoor and outdoor scenes with baselines reported in [8].

Indoor	PSNR \uparrow	SSIM \uparrow	LPIPS \downarrow
Plenoxels [32]	24.83	0.766	0.426
INGP-Base [15]	28.65	0.840	0.281
INGP-Big [15]	29.14	0.863	0.242
Mip-NeRF360 [14]	31.58	0.914	0.182
Baked-SDF [30]	27.06	0.836	0.258
3DGS [1]	30.41	0.920	0.189
SuGaR [8]	29.43	0.910	0.216
Ours	29.87	0.921	0.117
Outdoor	PSNR \uparrow	SSIM \uparrow	LPIPS \downarrow
Plenoxels [32]	22.02	0.542	0.465
INGP-Base [15]	23.47	0.571	0.416
INGP-Big [15]	23.57	0.602	0.375
Mip-NeRF360 [14]	25.79	0.746	0.247
Mobile-NeRF [29]	21.95	0.470	0.470
3DGS [1]	26.40	0.805	0.173
SuGaR [8]	24.40	0.699	0.301
Ours	24.61	0.719	0.262

a level set of the trained SDF function, as in [8]. Further refinement of the Gaussians can also be employed to improve the mesh quality by initializing a new set of Gaussians on the centers of the coarse mesh and jointly tuning the Gaussian as well as the mesh representation, which can end up being more computationally expensive. For our approach, we demonstrate that even with a shorter refining time, the mesh quality and rendering quality are not compromised when we run our computationally efficient regularizing for more iterations.

IV. RESULTS AND DISCUSSION

A. Implementation Details

All experiments were done using a NVIDIA RTX A6000 GPU. We follow the initial training regime in [8], performing 7000 iterations of vanilla GS, followed by 2000 iterations of opacity regularization. After this, we do either 6000, or 13000 iterations with our regularization. Depending on the number of regularizing iterations, we then have a refinement stage of either 15000 or 7000 iterations for a total of 30000 iterations. We use Omnidata [37] to generate the monocular normals.

B. Results

We compare the PSNR, SSIM, LPIPS [40] scores for various rendering datasets. Experiments were performed on the Tanks&Temples dataset [41] on the scenes *truck* and *train*. We also present results on the synthetic *Dr Johnson* and *Playroom* datasets from the Deep Blending repository [11]. Finally, we evaluate performance on realistic scenes from the MipNeRF360 [14], thus covering both indoor and outdoor scenes. We compare both with methods whose goal is to optimize rendering, and methods that extract meshes.

Note that in our experiments, GS sometimes performs better than our method in terms of photorealism metrics. This is not unexpected, and we emphasize that our goal is not necessarily to beat vanilla GS in terms of these metrics, but instead to produce scene representations that simultaneously

TABLE II: Results on the Tanks&Temples dataset with reported baseline values [8].

	PSNR \uparrow	SSIM \uparrow	LPIPS \downarrow
Plenoxels [32]	21.07	0.719	0.379
INGP-Base [15]	21.72	0.723	0.330
INGP-Big [15]	21.92	0.744	0.304
Mip-NeRF360 [14]	22.22	0.758	0.257
3DGS [1]	23.14	0.841	0.183
SuGaR [8]	21.58	0.795	0.219
Ours	21.83	0.802	0.216

TABLE III: Results on the Deep Blending dataset with reported baseline values [8].

	PSNR \uparrow	SSIM \uparrow	LPIPS \downarrow
Plenoxels [32]	23.06	0.794	0.510
INGP-Base [15]	23.62	0.796	0.423
INGP-Big [15]	24.96	0.817	0.390
Mip-NeRF360 [14]	29.40	0.901	0.244
3DGS [1]	29.41	0.903	0.242
SuGaR [8]	29.41	0.893	0.267
Ours	29.55	0.893	0.269
Ours (7K refinement)	29.72	0.894	0.277

perform well photorealistically while *also* being good for mesh generation - a feature lacking in standard GS. The closest work for comparison is SuGaR [8] which also proposes a modification to vanilla GS for better mesh generation.

Figure 2 demonstrates some of the images rendered using our method. For the MipNerF dataset we demonstrate competitive results with SoTA methods in rendering quality, and improve over the mesh-extracting methods (SuGaR, Baked-SDF, Mobile-NeRF) for both indoor and outdoor scenes. We report results for seven scenes from this dataset for our tests (all besides *Flowers* and *Treehill*) in Table I. For the Tanks&Temples dataset, our regularization improves over SuGaR in all metrics (Table II). Our regularization performs better than *all* other baselines for the Deep Blending dataset. On this dataset, we achieve a higher average PSNR than state-of-the-art methods (see Table III). We see that increasing the number of regularization iterations improves the quality of rendering but at the cost of a lower quality mesh for this dataset.

Figures 3 and 4 illustrate the UV-textured meshes extracted from the scenes, with triangle faces colored using the GS rasterizer, and the untextured meshes extracted from our method and vanilla GS, respectively. Both methods employ

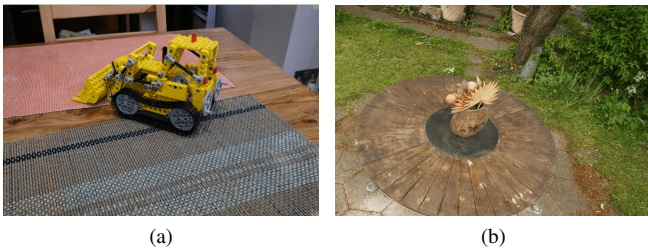


Fig. 2: Rendered images using our regularization.



Fig. 3: UV-Textured Meshes extracted after optimizing with our regularizing term, with colors rasterized onto the mesh.

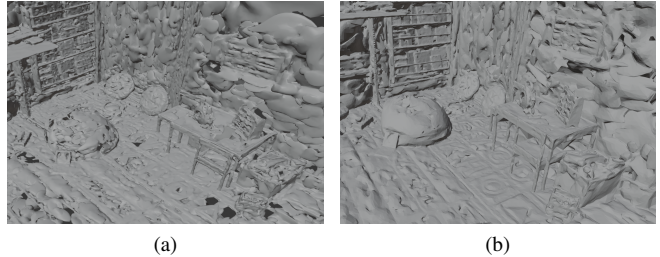


Fig. 4: Textureless meshes extracted from Gaussians (a) for vanilla GS and (b) after optimizing with our regularizing term for the scene in 3b. The 3DGS mesh contains holes, and is very noisy.

the same mesh-extraction technique from [8], but the vanilla GS mesh is noticeably noisy and contains holes. In Figure 5, we show the alignment of the estimated normals before and after adding the regularizing term. Clearly the method is able to denoise the normal estimation, and guide the Gaussians towards smoother geometric transitions.

That the rendering quality of our method can surpass that of 3D GS for some scenes is unsurprising because the regularizing term helps to place and align the Gaussians along regions of fine detail and texture.

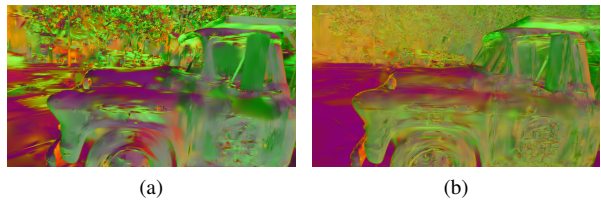


Fig. 5: Computed normals without and with regularization.

V. CONCLUSION

We introduce a novel regularization term for Gaussian splatting for geometrically accurate rendering and surface mesh extraction. We use a pre-trained neural network to predict per pixel monocular normals, that are then used to supervise the gradient of an estimated signed distance function whose zero level sets are the scene surface. We demonstrate improvement in the rendering quality while also extracting a surface mesh of the 3D scene.

REFERENCES

- [1] B. Kerbl, G. Kopanas, T. Leimkühler, and G. Drettakis, “3d gaussian splatting for real-time radiance field rendering,” *ACM Trans. Graph.*, vol. 42, no. 4, pp. 139–1, 2023.
- [2] B. Mildenhall, P. P. Srinivasan, M. Tancik, J. T. Barron, R. Ramamoorthi, and R. Ng, “Nerf: Representing scenes as neural radiance fields for view synthesis,” *Communications of the ACM*, vol. 65, no. 1, pp. 99–106, 2021.
- [3] G. Wu, T. Yi, J. Fang, L. Xie, X. Zhang, W. Wei, W. Liu, Q. Tian, and X. Wang, “4d gaussian splatting for real-time dynamic scene rendering,” in *Proceedings of the IEEE/CVF Conference on Computer Vision and Pattern Recognition*, 2024, pp. 20 310–20 320.
- [4] J. Tang, Z. Chen, X. Chen, T. Wang, G. Zeng, and Z. Liu, “Lgm: Large multi-view gaussian model for high-resolution 3d content creation,” in *European Conference on Computer Vision*. Springer, 2025, pp. 1–18.
- [5] L. Hu, H. Zhang, Y. Zhang, B. Zhou, B. Liu, S. Zhang, and L. Nie, “Gaussianavatar: Towards realistic human avatar modeling from a single video via animatable 3d gaussians,” in *Proceedings of the IEEE/CVF Conference on Computer Vision and Pattern Recognition*, 2024, pp. 634–644.
- [6] Z. Chen, F. Wang, Y. Wang, and H. Liu, “Text-to-3d using gaussian splatting,” in *Proceedings of the IEEE/CVF Conference on Computer Vision and Pattern Recognition*, 2024, pp. 21 401–21 412.
- [7] W. E. Lorensen and H. E. Cline, “Marching cubes: A high resolution 3d surface construction algorithm,” in *Seminal graphics: pioneering efforts that shaped the field*. ACM New York, NY, USA, 1998, pp. 347–353.
- [8] A. Guédon and V. Lepetit, “Sugar: Surface-aligned gaussian splatting for efficient 3d mesh reconstruction and high-quality mesh rendering,” in *Proceedings of the IEEE/CVF Conference on Computer Vision and Pattern Recognition*, 2024, pp. 5354–5363.
- [9] J. Flynn, I. Neulander, J. Philbin, and N. Snavely, “Deepstereo: Learning to predict new views from the world’s imagery,” in *Proceedings of the IEEE conference on computer vision and pattern recognition*, 2016, pp. 5515–5524.
- [10] T. Zhou, S. Tulsiani, W. Sun, J. Malik, and A. A. Efros, “View synthesis by appearance flow,” in *Computer Vision—ECCV 2016: 14th European Conference, Amsterdam, The Netherlands, October 11–14, 2016, Proceedings, Part IV 14*. Springer, 2016, pp. 286–301.
- [11] P. Hedman, J. Philip, T. Price, J.-M. Frahm, G. Drettakis, and G. Brostow, “Deep blending for free-viewpoint image-based rendering,” *ACM Transactions on Graphics (ToG)*, vol. 37, no. 6, pp. 1–15, 2018.
- [12] M. Niemeyer, J. T. Barron, B. Mildenhall, M. S. Sajjadi, A. Geiger, and N. Radwan, “Regnerf: Regularizing neural radiance fields for view synthesis from sparse inputs,” in *Proceedings of the IEEE/CVF Conference on Computer Vision and Pattern Recognition*, 2022, pp. 5480–5490.
- [13] A. Chen, Z. Xu, A. Geiger, J. Yu, and H. Su, “Tensorf: Tensorial radiance fields,” in *European conference on computer vision*. Springer, 2022, pp. 333–350.
- [14] J. T. Barron, B. Mildenhall, M. Tancik, P. Hedman, R. Martin-Brualla, and P. P. Srinivasan, “Mip-nerf: A multiscale representation for anti-aliasing neural radiance fields,” in *Proceedings of the IEEE/CVF international conference on computer vision*, 2021, pp. 5855–5864.
- [15] T. Müller, A. Evans, C. Schied, and A. Keller, “Instant neural graphics primitives with a multiresolution hash encoding,” *ACM transactions on graphics (TOG)*, vol. 41, no. 4, pp. 1–15, 2022.
- [16] P. Wang, L. Liu, Y. Liu, C. Theobalt, T. Komura, and W. Wang, “Neus: Learning neural implicit surfaces by volume rendering for multi-view reconstruction,” *arXiv preprint arXiv:2106.10689*, 2021.
- [17] Z. Yu, S. Peng, M. Niemeyer, T. Sattler, and A. Geiger, “Monosdf: Exploring monocular geometric cues for neural implicit surface reconstruction,” *Advances in neural information processing systems*, vol. 35, pp. 25 018–25 032, 2022.
- [18] A. Gropp, L. Yariv, N. Haim, M. Atzmon, and Y. Lipman, “Implicit geometric regularization for learning shapes,” *arXiv preprint arXiv:2002.10099*, 2020.
- [19] Y. Ben-Shabat, C. H. Koneputugodage, and S. Gould, “Digs: Divergence guided shape implicit neural representation for unoriented point clouds,” in *Proceedings of the IEEE/CVF Conference on Computer Vision and Pattern Recognition*, 2022, pp. 19 323–19 332.
- [20] R. Wang, Z. Wang, Y. Zhang, S. Chen, S. Xin, C. Tu, and W. Wang, “Aligning gradient and hessian for neural signed distance function,” *Advances in Neural Information Processing Systems*, vol. 36, 2024.
- [21] D. Rückert, L. Franke, and M. Stamminger, “Adop: Approximate differentiable one-pixel point rendering,” *ACM Transactions on Graphics (ToG)*, vol. 41, no. 4, pp. 1–14, 2022.
- [22] C. Lassner and M. Zollhofer, “Pulsar: Efficient sphere-based neural rendering,” in *Proceedings of the IEEE/CVF Conference on Computer Vision and Pattern Recognition (CVPR)*, June 2021, pp. 1440–1449.
- [23] M. Zwicker, H. Pfister, J. Van Baar, and M. Gross, “Ewa splatting,” *IEEE Transactions on Visualization and Computer Graphics*, vol. 8, no. 3, pp. 223–238, 2002.
- [24] Z. Yu, A. Chen, B. Huang, T. Sattler, and A. Geiger, “Mip-splatting: Alias-free 3d gaussian splatting,” in *Proceedings of the IEEE/CVF Conference on Computer Vision and Pattern Recognition*, 2024, pp. 19 447–19 456.
- [25] T. Lu, M. Yu, L. Xu, Y. Xiangli, L. Wang, D. Lin, and B. Dai, “Scaffold-gs: Structured 3d gaussians for view-adaptive rendering,” in *Proceedings of the IEEE/CVF Conference on Computer Vision and Pattern Recognition*, 2024, pp. 20 654–20 664.
- [26] J. C. Lee, D. Rho, X. Sun, J. H. Ko, and E. Park, “Compact 3d gaussian representation for radiance field,” in *Proceedings of the IEEE/CVF Conference on Computer Vision and Pattern Recognition*, 2024, pp. 21 719–21 728.
- [27] S. Girish, K. Gupta, and A. Shrivastava, “Eagles: Efficient accelerated 3d gaussians with lightweight encodings,” *arXiv preprint arXiv:2312.04564*, 2023.
- [28] S. Fridovich-Keil, A. Yu, M. Tancik, Q. Chen, B. Recht, and A. Kanazawa, “Plenoxels: Radiance fields without neural networks,” in *Proceedings of the IEEE/CVF conference on computer vision and pattern recognition*, 2022, pp. 5501–5510.
- [29] Z. Chen, T. Funkhouser, P. Hedman, and A. Tagliasacchi, “Mobilenerf: Exploiting the polygon rasterization pipeline for efficient neural field rendering on mobile architectures,” in *Proceedings of the IEEE/CVF Conference on Computer Vision and Pattern Recognition*, 2023, pp. 16 569–16 578.
- [30] L. Yariv, P. Hedman, C. Reiser, D. Verbin, P. P. Srinivasan, R. Szeliski, J. T. Barron, and B. Mildenhall, “Baked sdf: Meshing neural sdf for real-time view synthesis,” in *ACM SIGGRAPH 2023 Conference Proceedings*, 2023, pp. 1–9.
- [31] M. Turkulainen, X. Ren, I. Melekhov, O. Seiskari, E. Rahtu, and J. Kannala, “Dn-splatter: Depth and normal priors for gaussian splatting and meshing,” *arXiv preprint arXiv:2403.17822*, 2024.
- [32] K. Zhang, F. Luan, Q. Wang, K. Bala, and N. Snavely, “Physg: Inverse rendering with spherical gaussians for physics-based material editing and relighting,” in *Proceedings of the IEEE/CVF Conference on Computer Vision and Pattern Recognition*, 2021, pp. 5453–5462.
- [33] J. Choi, Y. Lee, H. Lee, H. Kwon, and D. Manocha, “Meshgs: Adaptive mesh-aligned gaussian splatting for high-quality rendering,” *arXiv preprint arXiv:2410.08941*, 2024.
- [34] J. Waczyńska, P. Borycki, S. Tadeja, J. Tabor, and P. Spurek, “Games: Mesh-based adapting and modification of gaussian splatting,” *arXiv preprint arXiv:2402.01459*, 2024.
- [35] J. Gao, C. Gu, Y. Lin, H. Zhu, X. Cao, L. Zhang, and Y. Yao, “Relightable 3d gaussian: Real-time point cloud relighting with brdf decomposition and ray tracing,” *arXiv preprint arXiv:2311.16043*, 2023.
- [36] J. L. Schonberger and J.-M. Frahm, “Structure-from-motion revisited,” in *Proceedings of the IEEE conference on computer vision and pattern recognition*, 2016, pp. 4104–4113.
- [37] A. Eftekhar, A. Sax, J. Malik, and A. Zamir, “Omnidata: A scalable pipeline for making multi-task mid-level vision datasets from 3d scans,” in *Proceedings of the IEEE/CVF International Conference on Computer Vision*, 2021, pp. 10 786–10 796.
- [38] R. Ranftl, K. Lasinger, D. Hafner, K. Schindler, and V. Koltun, “Towards robust monocular depth estimation: Mixing datasets for zero-shot cross-dataset transfer,” *IEEE transactions on pattern analysis and machine intelligence*, vol. 44, no. 3, pp. 1623–1637, 2020.
- [39] M. Kazhdan, M. Bolitho, and H. Hoppe, “Poisson surface reconstruction,” in *Proceedings of the fourth Eurographics symposium on Geometry processing*, vol. 7, no. 4, 2006.
- [40] R. Zhang, P. Isola, A. A. Efros, E. Shechtman, and O. Wang, “The unreasonable effectiveness of deep features as a perceptual metric,” in *Proceedings of the IEEE conference on computer vision and pattern recognition*, 2018, pp. 586–595.
- [41] A. Knapitsch, J. Park, Q.-Y. Zhou, and V. Koltun, “Tanks and temples: Benchmarking large-scale scene reconstruction,” *ACM Transactions on Graphics (ToG)*, vol. 36, no. 4, pp. 1–13, 2017.